Plasma functionalization of AFM tips for measurement of chemical interactions

Cedric Volcke[1,2,*], Ram Prasad Gandhiraman[1], Vladimir Gubala[1], Colin Doyle[3], G. Fonder[4], Paul A. Thiry[2], Attilio A. Cafolla[1,5], Bryony James[3] and David E. Williams[1,6]

[1] Biomedical Diagnostics Institute (BDI), Dublin City University, Collins Avenue, Glasnevin, Dublin 9, Ireland.
[2] Research Centre in Physics of Matter and Radiation (PMR), University of Namur (FUNDP), 61 rue de Bruxelles, B-5000 Namur, Belgium.
[3] Research Centre for Surface and Materials Science, Department of Chemical and Materials Engineering, University of Auckland, Private Bag 92019, Auckland 1142, New Zealand.
[4] Laboratory of Chemistry and Electrochemistry of Surfaces (CES), University of Namur (FUNDP), 61 Rue de Bruxelles, B-5000 Namur, Belgium.
[5] School of Physics, Dublin City University, Collins Avenue, Glasnevin, Dublin 9, Ireland.
[6] MacDiarmid Institute for Advanced Materials and Nanotechnology, Department of Chemistry, University of Auckland, Private Bag 92019, Auckland 1142, New Zealand

ABSTRACT

In this paper, a new, fast, reproducible technique for atomic force microscopy (AFM) tips functionalization used for chemical interaction measurements is described. Precisely, the deposition of an aminated precursor is performed through plasma enhanced chemical vapour deposition (PECVD) in order to create amine functional groups on the AFM tip and cantilever. The advantages of the precursor, aminopropyltriethoxysilane (APTES), were recently demonstrated for amine layer formation through PECVD deposition on polymeric surfaces. We extended this procedure to functionalize AFM probes. Titration force spectroscopy highlights the successful functionalization of AFM tips as well as their stability and use under different environmental conditions.

Keywords: Force spectroscopy, Amine, PECVD, Titration force spectroscopy

* To whom correspondence should be addressed. E-mail : cedric.volcke@fundp.ac.be

Introduction

During the last two decades, scanning probe microscopies (SPM) progressively became essential techniques in a variety of domains, ranging not only from chemistry [1], surface physics [2] to biology [3] but also food and agricultural research [4], biomedical and biosensor devices [5], or pharmaceutical industry [6]. Originally composed of two members, i.e. scanning tunnelling microscope (STM) and atomic force microscope (AFM) [7], the SPM family rapidly extended through the development of AFM derived techniques such as amongst others: lateral force microscopy (LFM) [8], chemical force microscopy (CFM) [9], electric and magnetic force microscopy (EFM and MFM) [10], force spectroscopy (FS) [11], kelvin probe force microscopy (KFM) [12], molecular recognition force microscopy (MRFM) [13-14]...

Some of those techniques are providing chemical and biological informations through judicious use of chemical and biological interactions. For example, appropriate functionalization of STM tips was previously used to identify functional groups inside molecules organized in self-assembled monolayers at liquid-solid interfaces [15]. Similar technique discriminates bases in DNA molecules [16]. In atomic force microscopy derivative such probe modifications were extensively used to identify and quantify chemical and biological interactions [17]. For example, chemical force microscopy reveals specific chemical functionality at the nanoscale by using chemically modified AFM probes [18]. In such a case, hydrogen-bonding and/or hydrophobic interactions are governing the probe-surface interaction, providing chemical contrast in the resulting SPM images. In molecular recognition force microscopy, attachment of antibody at the tip apex allowed the identification and localisation of recognition events between antibody on the probe and antigens deposited at surfaces [14].

Generally, those AFM probe modifications require the presence of functional groups like carboxylic or amino groups at the tip apex. The attachment of alkanethiol self-assembled monolayers (SAMs) onto gold (or platinum) coated AFM probes is the most commonly used probe modification technique [19]. However, this latter procedure is detrimental to some important experimental parameters such as tip radius of curvature, for example. Moreover, alkanethiol SAMs formation on gold coated AFM probes is mostly performed in liquid-phase. Such procedure may use hazardous materials producing liquid wastes environmentally non friendly. Also, these are relatively time-consuming. Finally, SAMs stability may reduce probe lifetime. Organosilane functionalization of silicon or silicon nitride tips is another possibility although not really explored [20]. This can originate from the fact that liquid-phase deposition of silane is well-known to produce fairly thick polymeric layer.

In such cases, gas-phase deposition process can be a good alternative. Although not exposed in literature, it resolves major issues arising from liquid-phase deposition process. Particularly, plasma enhanced chemical vapour deposition (PECVD) retained our attention. Indeed, it is a versatile surface engineering technique which had proven to be an excellent tool for surface modification and large scale industrial production [21]. Moreover, it enables rapid, low-temperature deposition of various functional groups in a controlled way on a large variety of substrates including complex three-dimensional structures [22]. In this technique, a plasma discharge is created in presence of a precursor containing the required chemical groups. The deposited coatings are uniformly dispersed, with a precise control on thickness.

This technique has previously been used to modify substrates such as glass, silicon or polymers in order to monitor their surface properties. For example, hexamethyldisiloxane

(HMDSO) PECVD deposited coatings were used to tailor hydrophilic property of polymeric surfaces [23]. Also, amino-functionalization of surfaces has previously been demonstrated using PECVD from ethylene diamine (EDA) or allylamine precursor on glass, silicon or polypropylene [24-25]. Recently, an alternative precursor, (3-aminopropyl)triethoxysilane (APTES), was highlighted as appropriate for cycloolefin copolymers amination [26-27]. Due to the presence of Si-O groups this molecule is creating chemical bonding to plasma activated surfaces, allowing a good adhesion, stability and high amino-content of the coating.

However, up to now, PECVD deposition of aminated precursor on AFM probes in order to functionalize them for chemical applications (as CFM or FS) was not explored. In this paper, we propose to fill this gap by demonstrating the amino functionalization of AFM probes through PECVD deposition of APTES precursor. The coating is first characterised using X-ray photoelectron spectroscopy (XPS), ellipsometry, dual polarization interferometry (DPI), water contact angle (WCA) measurements and AFM imaging. The probe functionalization and coating stability is analyzed through chemical force spectroscopy and chemical force titration measurements.

Materials and Methods

Materials

3-aminopropyltriethoxysilane (APTES), hydrochloric acid (HCl), high purity HPLC grade water and sodium hydroxide (NaOH) were purchased from Sigma Aldrich and used without further treatment. Hyperpure silicon polished (100) n-doped silicon substrates were provided by Wacker Chemitronic GmbH.

The PECVD system

The experiment was carried out in a computer controlled PECVD reactor Europlasma, model CD300 (Oudenaarde, Ghent, Belgium). An aluminium vacuum chamber, connected to a Dressler's CESAR 136 RF power source (Munsterau, Stolberg, Germany) with an operating frequency of 13.56 MHz with an automated match-box was used. The chamber details are described elsewhere [22, 23, 28]. The AFM probes were placed at a floating electrode and the input power was fixed at 14 watt. The powered electrode, a 24 cm x 21 cm plate with a 6 cm diameter hole in the middle, was placed slightly below the top of the chamber and the chamber wall was grounded. The powered electrode is cooled with running water. Also a 24 cm x 21 cm x 1.2 cm electrically isolated, water cooled hollow metallic setup placed 10 cm away from the powered electrode is used as the substrate holder. The powered electrode (PE) is separated from the ground chamber by ceramic spacers and a floating potential (FP) electrode is placed under the powered electrode. The APTES precursor was stored in a KF25 closed nipple connected to the chamber through a needle valve. The needle valve was used to control the flow of precursor APTES vapors. As the vapor pressure of APTES is less than 10 Torr at 1000° C, the APTES container was heated at 80° C and to prevent condensation of

APTES in pipelines, the stainless steel supply lines from source to vacuum chamber were also heated at 80° C through a temperature controlled heating tape.

Surface preparation

AFM probes and silicon plates were first cleaned with dry air before being loaded in the plasma chamber. The chamber was pumped down to a base pressure of 20 mTorr. Prior to the deposition, plasma cleaning and activation was carried out using argon (50 sccm) + oxygen (50 sccm) mixed plasma (250 watt RF power). After three minutes, the oxygen flow was closed and the RF power reduced to 14 watt. APTES is then introduced in the chamber during the required deposition time of 30 seconds. A short deposition time was used because a very thin coating was required. The operating pressure is ~ 70 mTorr. The APTES supply is then closed and plasma RF power shut down.

Surface characterization

Ellipsometry

The thickness of the APTES coating on silicon wafer was characterized using J.A. Woollam Co., Inc EC-400, M-2000UI Spectroscopic Ellipsometer. All layers were modeled as a simple silicon dioxide dispersion layer to extract an effective thickness.

Contact angle

The film wettability is analysed by measuring the water contact angle (WCA) of the film surface using a VCA 2500 XE contact angle meter on a 2.5 µl solution drops that were allowed to equilibrate at room temperature in ambient atmoqphere during 15 to 30 s. Water used in these experiments was deionised (18 MΩ cm resistivity) with a Millipore Milli-Q filtration system. Unbuffered, constant low ionic-strength solutions (10^{-2} M) of HCl and NaOH were freshly prepared and used to control the pH. Mean contact angle values obtained

on 3 differents measurements at different places on the sample surface. Experiments were reproduced at least 3 times on several samples.

Atomic force microscopy imaging (AFM)

AFM examinations are performed in ambient air with a commercial microscope (Dimension 3100 controlled by a Nanoscope IIIa controller, Digital Instruments, Santa-Barbara – CA, USA), in the Tapping-Mode™, using standard unmodified silicon cantilevers (BudgetSensors®, Bulgaria) with a 7 nm radius of curvature and a 42 $N.m^{-1}$ spring constant (nominal values). Topographic images are recorded at a scanning rate of 1-2 Hz, and a resonance frequency of about 300 kHz (nominal value). The background slope is resolved using first order polynomial function. No further filtering is performed. The surface roughness of silicon substrates and PECVD deposited APTES layer on silicon substrate is evaluated over 3 images (2 µm x 2 µm) and the standard deviation is then calculated. The root-mean-square roughness (Rrms) considered is defined as the average of height deviations taken from the mean plane [29].

X-ray photoelectron spectroscopy (XPS)

The XPS data were collected on a Kratos Axis UltraDLD equipped with a hemispherical electron energy analyser. Spectra were excited using monochromatic Al Kα X-rays (1486.69 eV) with the X-ray source operating at 100 W. This instrument illuminates a large area on the surface and then using hybrid magnetic and electrostatic lenses collects photoelectrons from a desired location on the surface. In this case the analysis area was a 220 µm by 220 µm spot. The measurements were carried out in normal emission geometry. Survey scans were collected with 160 eV pass energy, whilst core level scans were collected with pass energy of

20 eV. The analysis chamber was at pressures in the 10^{-9} Torr range throughout the data collection.

Data analysis was performed using CasaXPS (www.casaXPS.com). Shirley backgrounds were used in the peak fitting. Quantification of survey scans utilised relative sensitivity factors supplied with the instrument. Core level data were fitted using Gaussian-Lorentzian peaks (30 % Lorentzian). The elements present in the coating C, N, O, Si were detected using the XPS survey scan, (Supporting informations). High resolution scans of individual core levels show the various bonding states.

Chemical Force Titration (CFT)

Commercial triangular silicon nitride cantilevers (BudgetSensors®, Bulgaria) with 0.06 N/m spring constant and 7 nm radius of curvature (nominal values) were functionalized by APTES molecules through PECVD deposition process as described above. Water used in these experiments was deionised (18 MΩ cm resistivity) with a Millipore Milli-Q filtration system. Unbuffered, constant low ionic-strength solutions (10^{-2} M) of HCl and NaOH were freshly prepared and used to control the pH. The probe tips and functionalized surfaces were immersed in a droplet of a given pH solution.

The force measurements were performed on a commercial microscope (MultiMode AFM equipped with a Nanoscope IIIa electronics and a liquid cell, Digital Instruments, Santa-Barbara, CA). Adhesion force values were obtained from ~ 100 force-distance curves per pH value in several different places on the sample. Each force-distance curve was obtained with a Z scan size of ~ 500 nm and a scan rate of 1 cycle/s. All measurements were made using the same AFM probe. Measurements were made by alternating from high to low and from low to high pH to check the stability of the surface and the tip as a function of time. The tip and

substrate were rinsed with deionized water and dried in a stream of nitrogen before each pH change. Experiments were reproduced at least 3 times on several samples. The pull-off force values were calculating using the Scanning Probe Image Processor software (SPIP™, Image Metrology). Averaged adhesion values were determined from Gaussian fits on histograms of the adhesion values obtained from ~ 100 individual force-versus-distance curves, and the reported errors correspond to the standard deviations.

Dual Polarization Interferometry (DPI)

The dual polarization interferometry, an optical sensing technique was carried out using a Farfield AnaLight® instrument. The surface used was a silicon oxynitride AnaChip™ and the temperature was controlled throughout to 20° C. The structural changes taking place with the addition of a surfactant are investigated by monitoring the refractive index, thickness and mass variations with the addition of PBS Tween®. The Silicon oxynitride AnaChip™ consists of two optical waveguides that confine light into defined boundaries, one stacked on top of the other separated by an insulated layer. The substrate is silicon wafer and the waveguides are silicon dioxide doped with silicon nitride. A collimated light beam from a helium-neon laser (wavelength 632.8 nm) is first passed through a ferroelectric liquid crystal ½ wave plate to create plane polarized light. The liquid crystal is switched such that during one half of the measurement transverse magnetic phase is passed through the waveguide and during the other half measurement transverse electric phase is passed through. When the laser beam is passed through the edge of the sensor chip, it propagates through both waveguides. The two beams diverge and form a Young's interference pattern at the side of the chip in far-field. The top wave guide that is exposed to the analyte is a sensing waveguide and the speed of the light travelling through it will change if the molecules are attached or removed from it. The light travelling through the bottom waveguide is unaffected and progresses at a constant

velocity and it acts as an optical reference. The interference pattern represents the relative phase position of the upper and lower modes at the output face of the device. The precise positions of the light and dark bands depend upon the phase relationship of the light as it emerges from the two waveguides. An addition or removal of material from the top surface of the sensing waveguide would result in a shift of the interference fringe position. The phase change is due to a variation in the top sensing waveguide. As the refractive index of the lower reference waveguide is unaffected, the phase shift is related solely to the change observed in the sensing waveguide. Based on the details of the phase shift, a range of layer thicknesses and refractive index values can be calculated.

Results and discussions

Coating characteristics

APTES coatings were first deposited on silicon substrates through PECVD deposition under 14 watt RF plasma power and 30 s deposition time. The mean coating thickness is about 5.2 nm, as measured by ellipsometry. Concerning the coating thickness on the AFM probe, as we did not find a way to directly measure it, we simply assumed that the characteristics of the coating on the tip are very close to the same coating deposited on a silicon wafer. This assumption is also considered for coating hydrophilicity measurements. In such a case, water contact angle (WCA) is around 54° ± 1, a value similar to that found in literature for liquid-phase deposited APTES on silicon oxide surfaces, as well as APTES PECVD deposited on polymeric surfaces [26-27, 30]. This change in film wettability is a confirmation of successful surface chemistry modification.

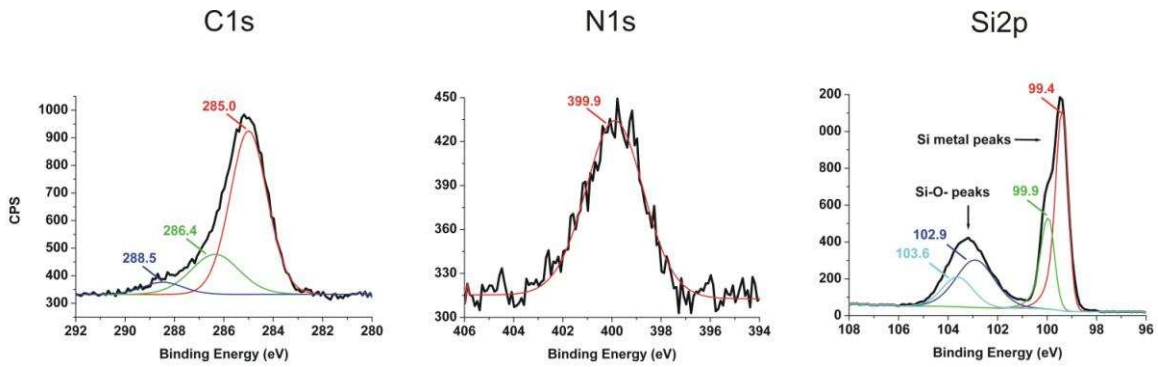

Figure 1. High resolution core level photoemission spectra of (a) C 1s (b) N 1s (c) Si 2p, taken with a pass energy of 20 eV using monochromatic Al Kα monochromatic X-rays (1486.69 eV), with the X-ray source operating at 100 W. The analysis area was a 220 by 220 micron spot. The measurements were carried out in normal emission geometry. The core level peaks are deconvoluted to show the various bonding environments. Data analysis was performed using CasaXPS (www.casaXPS.com). Shirley backgrounds were used in the peak fitting. Core level data were fitted using Gaussian-Lorentzian peaks (30 % Lorentzian).

The chemical composition of coatings is determined through X-ray photoelectron spectroscopic analysis (Fig. 1). The presence of carbon, oxygen, silicon and nitrogen species in the coating is highlighted in the XPS survey spectrum (Supporting Informations). Qualitatively, the C1s spectrum (Fig. 1, left) was deconvoluted with three main contributions: at 285.0, 286.4 and 288.5 eV, which are attributed to aliphatic carbon, C-N and C-O-NH_2 species, respectively [31]. The N1s region highlights one peak centred at 399.9 eV and can be attributed to the presence of NH_2 groups (Fig. 1, centre) [31]. The Si2p spectrum is deconvoluted using 4 contributions: two associated to pure silicon ($Si2p_{1/2}$ at 99.4 eV and $Si2p_{3/2}$ at 99.9 eV) and two associated to silicon oxide Si-O- ($Si2p_{1/2}$ at 103.6 eV and $Si2p_{3/2}$ at 102.9 eV) (Fig. 1, right) [31]. The observation of signals attributable to elemental Si, the substrate, implies that, at least in parts over the surface, the coating was of thickness commensurate with the escape depth of the photoelectrons: a few nm at most. Moreover, the nitrogen/carbon ratio extracted from XPS data (0.12) is almost identical to the N/C ratio of the monomer (0.11). Thus, the coating can be expected to present a significant number of hydrophilic amino groups at the surface in addition to hydrocarbon fragments, as confirming WCA data.

The interfacial coating properties were analyzed using DPI. By defining the waveguide structure with alternate polarizations both the refractive index and the thickness of adsorbed layers at the substrate (solid) – liquid interface were determined. Information about the mass and the density of the film was derived, based on which the amount of amino groups for each sample was calculated, assuming that the silane does not fragment but retains its molecular identity. Therefore, from the mass of the film per cm^2 and the molar mass of the monomer, the number of moles of $–NH_2$ in the film per cm^2 of geometric area can be calculated. DPI allowed monitoring the layer composition of the coated slide before and after a treatment with

1% w/v solution of PBS Tween (PBST) to probe the film adhesion and the structural changes upon washing with a detergent. This technique revealed that the APTES coatings undergo a small swelling when in contact with PBS buffer, which is reflected in the increased thickness of the layer from 5.12 to 6.39 nm. PBS Tween treatment leaves the APTES film virtually unaffected, keeping the APTES mass constant at 3.80 ng / mm^2. The averaged number of amino groups is estimated around 16.7 × 10^{14} /cm^2 before and after treatment with PBS Tween® [27]. This value is about 3-4 times higher than what is observed for APTES layers deposited through traditional liquid-phase technique on silicon substrates [25, 32]. We can also notice that the coating height measure through ellipsometry (5.2 nm) and DPI (5.12 nm) experiments are in very good agreement, highlighting the reproducibility of the deposition process.

Stability/change in coating surface structure in liquids is checked through AFM imaging. Tapping-Mode™ topographical (TM-AFM) images were performed in air, under DI water and under PBS Tween®**.** As observed in Fig. 2A, APTES coating in air exhibits globular structures in the range of 50-200 nm in diameter and below 10 nm in height. These structures can originate from polymerisation of APTES molecules on the silicon surface. This fact is usually observed while water is present during the liquid-phase deposition process. Here, the APTES precursor is not 100% anhydrous and also it is exposed to atmosphere while transferring to the source container, which could have resulted in absorption of moisture content from atmosphere. This could therefore lead to the formation of the observed structures. The surface roughness (rms) is measured as being ~ 1.2 nm. However, while imaged under DI water, the same surface appears more flat and homogeneous with a mean roughness around 0.7 nm (Fig. 2B). Swelling of the surface, as also deduced from DPI data, can explain these surface modifications. Unbound, physisorbed APTES molecules (or fragments), washed away by the water environment, can also explain the disappearing of the

globular features. While imaged under PBS Tween® environment (Fig. 2C), APTES coating are also revealing globular structures. However, these ones appears bigger (200-400 nm in diameter) and more dispersed. Their heights are still below 10 nm, rendering a mean roughness value around 0.9 nm.

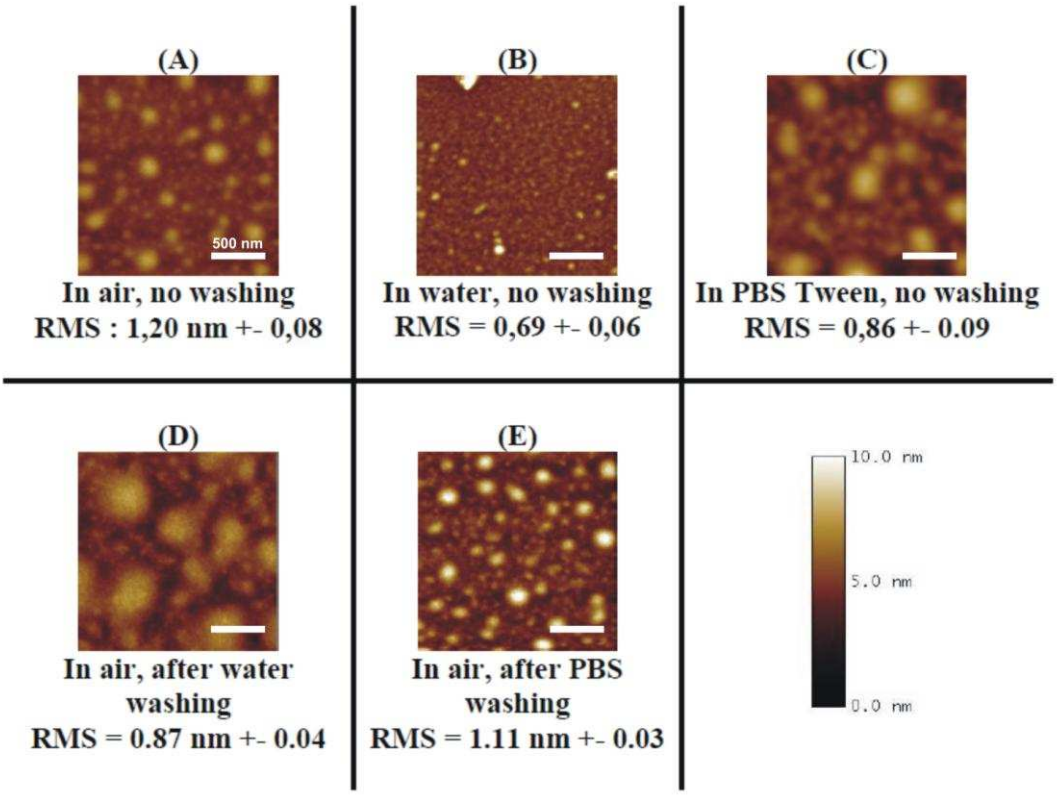

Figure 2. Tapping-Mode AFM topographical imaging (2 µm x 2 µm) of PECVD deposited APTES coating on silicon wafer in diverse environment: (A) in air, (B) in DI water, (C) in PBS Tween®, (D) in air after washing with DI water and drying in air, (E) in air after washing with PBS Tween® and drying in air. RMS roughness values are also indicated. (Bottom right) Z-scale color bar.

In order to determine the origin of such surface topographical changes, some more experiments were performed. Imaging is done in air, before and after washing with DI water and PBS Tween® (Figs 2D and 2E, respectively). A water wash and an imaging in air after drying reveals globular structures (Fig. 2D). Their characteristics are about 300-500 nm in diameter and around 3 nm in height. Washing with water and blow drying with N_2 flow could

have resulted in removal of partly or loosely bound particles. The change in film density with removal of molecules could result in a significant change in morphology. A swelling effect due to residual and or atmospheric water on the surface is again privileged in order to explain the observed globular structures, although a non-significant polymerization effect can not totally be discarded.

After a PBS Tween® treatment, the coating surface still presents globular structures (100-200 nm in diameter and 5-7 nm in height) (Fig. 2E). Those observations also correlate to a swelling of the deposited coating. However, it appears to be less pronounced than in water due to presence of ions in solution, probably getting tendency to get attached to the structures. Also, the presence of Tween®, acting as a detergent, in the PBS solution could result in the decreased size of globular structures at the coating surface after PBS-Tween® washing.

At this stage, we can therefore confirm the deposition of an APTES coating (~ 5.2 nm thick), presenting a high density of surface amino groups, fairly stable and reproducible. Moreover, coating surface roughness is relatively small in water, making those appropriate for chemical force microscopy measurements in aqueous solutions while deposited onto AFM probes.

Application to chemical force titration

In order to check the efficient functionalization of the three-dimensional AFM probes by PECVD deposition of APTES precursor, and also to demonstrate their applicability to chemical interaction measurements, chemical force titration experiments were performed. In such "force titration" measurements, the chemical adhesion (under liquid environment) between a modified AFM tip and a similarly modified sample surface is monitored as a function of the solution pH.

By performing pH dependent force-distance curves, the contribution of the ionisable functional groups, i.e., amino groups can be studied separately. In aqueous solutions, the sum of the different attractive forces is counteracted by the electrostatic repulsion of protonated amino groups if pH is close to or lower than the pK_a of these groups. Thus, in such systems, the balance between attractive forces and repulsive electrostatic forces is measured as a force-distance curve. This technique has previously been used to characterize the interactions between tips and sample substrates modified with carboxylic acid, amine and phosphonic acid groups [33-38]. Most of those studies focused on systems in which both tip and samples were functionalized by liquid phase deposition using alkanethiols on gold, for example. We propose to use our modified probe with this technique. Experiments were performed at fixed ionic strength, as it is known to drastically modify forces measured [33, 36-37, 39]. To ensure the comparability of the data obtained at different pH solutions, one tip was used throughout one set of force titration experiments. Experiments are then reproduced different times with different tips.

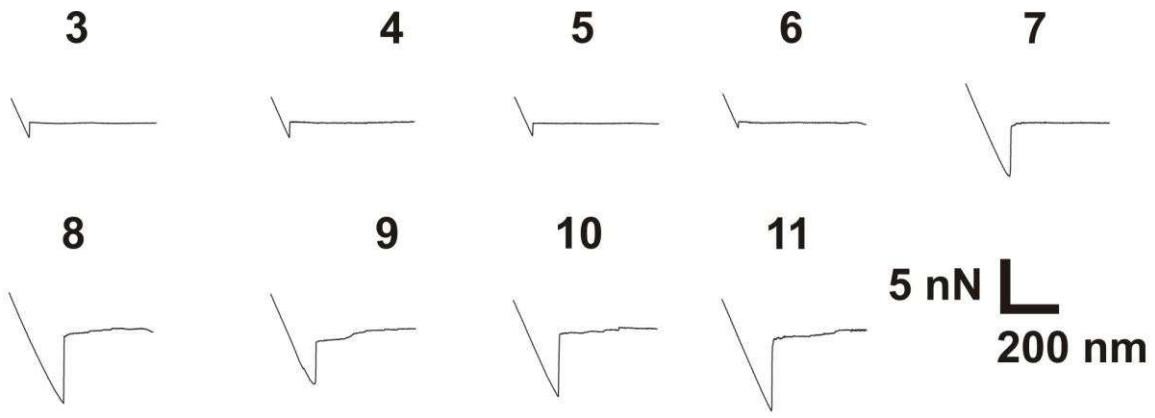

Figure 3. Representative retraction force curves for NH_2 terminated tips and NH_2 modified substrate surface in different pH solutions. Upper number indicates pH of the solution during experiment.

Fig.3 shows typical retraction force curves between APTES plasma modified AFM tip and similarly modified silicon surfaces at different pH between 3 and 11 in fixed 10^{-2} M ionic

strength solutions. Pull-on (black) as well as pull-off forces (red) clearly highlight variations with pH. In this paper, we only focus on pull-off forces (adhesion forces) measured through retraction force curves.

Average adhesion force values obtained at different solution pH values (~ 100 individual force measurements for each pH value, obtained at three different positions on sample surface) for tip and sample functionalized with PECVD deposited APTES are plotted in Fig. 4. In these averaged pH-dependent force measurements, a pronounced dependence of the magnitude of the averaged pull-off forces on the pH was highlighted. An increase in adhesive force with increasing pH is observed. The averaged pull-off force exhibits behaviour similar to conventional titration experiments and is consistent with protonation/deprotonation of amine groups on both surfaces. Precisely, at low pH values, the repulsive interaction may arise from the long-range electrostatic interaction between protonated NH_2 groups on tip and sample surface (as schemed in Fig. 4). Oppositely, at higher pH values, the attractive interaction observed may originate from van der Waals and hydrogen interactions between neutral surface NH_2 groups. Vand der Waals interactions can be considered as constant with varying pH and are contributing to the non-zero adhesion force measured at low pH values.

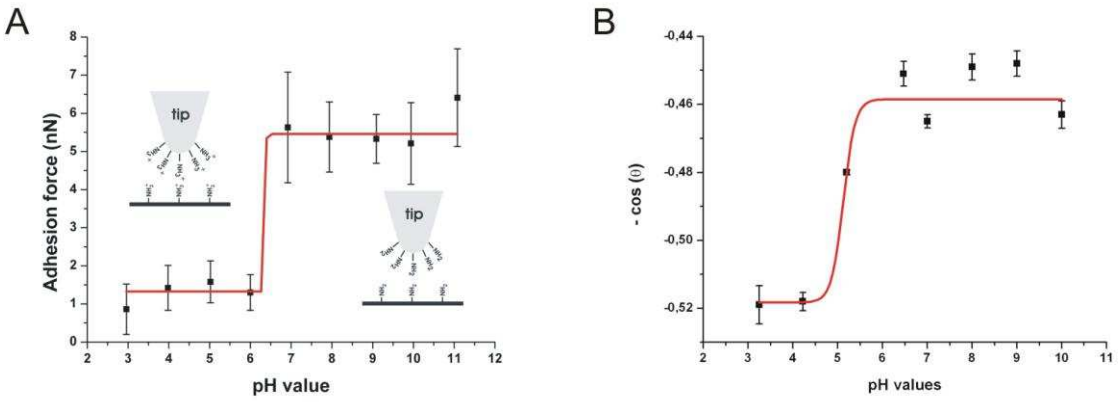

Figure 4. (A) Chemical force titration curve for tip and surface both modified with PECVD deposited APTES coating, acquired under solution of 10^{-2} M ionic strength. (The curve has been added as a guide to the eye). Scheme are presenting the proposed interactions of APTES modified tips and APTES modified surface in water at different pH values. (B) Negative cosine of the averaged contact angles of water drops on a silicon surface modified with PECVD deposited APTES as a function of pH.

For comparison, we have performed contact angle titration experiments using water solution droplets of various pH values on the PECVD deposited APTES coating on silicon surface. Figure 4B exhibits the contact angle titration curve, in which 3 different measurements were performed for each pH value to obtain the mean contact angle. The contact angle remained almost stationary above pH 6.0. These data also show a sharp transition (an increase in wettability) as the droplet pH is reduced below from pH 6.0 to 4.0. An increase in wettability is expected while surface becomes more protonated. Finally contact angle became constant at pH 4.0 and below. The pKa value of this surface can be estimated at 5.2.

The measured adhesive forces, as presented in Fig. 4, can be used to calculate the local degree of ionization α_I and the acid dissociation constant value pK_a extracted from it. Indeed, as theoretically described in literature [40], interaction forces between tip and surface can reasonably been described with the Johnson, Kendall, Roberts model of adhesion mechanics, known as JKR model [41]. They described the pull-off force between a sphere 1 (modelling the AFM tip) and a flat surface 2 (modelling the sample surface) in a medium 3 as:

$$F_{adh} = -(3/2)\ \pi R\, W_{12}$$

with R, the AFM tip radius of curvature and W_{12} is the work of adhesion needed to pull the tip off the sample surface. The work of adhesion W_{12} can be expressed in term of γ_{13} (the tip-surface free energy in equilibrium with the medium), γ_{23} (the substrate-surface free energy in equilibrium with the medium) and γ_{12} (the interfacial free energy of the tip-substrate interface) such as: $W_{12} = \gamma_{13} + \gamma_{23} - \gamma_{12}$. If tip and sample surface are identically functionalized (with NH_2 groups for example), the work of cohesion can be expressed as $W_{12} = 2\ \gamma_{LS}$, where $\gamma_{LS} = \gamma_{13} = \gamma_{23}$ is the surface free energy of the particular surface functionality against the medium, the interfacial free energy γ_{12} being zero. Moreover, the degree of ionization of surfacial amine functional groups is given by the relationship:

$$\alpha_i = [NH_3^+] / ([NH_3^+] + [NH_2])$$

If we assume that changes in γ_{LS} ($\delta\gamma_{LS}$) with pH variations only depend linearly on the fraction of amino groups NH_2 converted to NH_3^+, the degree of ionization α_i can be related to γ_{LS} at limiting values of pH(x) for which the surface is fully protonated (pH(3)) and completely ionized (pH(11)). As γ_{LS} is directly proportional to the measured adhesion force, we can finally describe α_i as:

$$\alpha_i\,(pH(x)) = [F_{adh}(pH(3)) - F_{adh}(pH(x))] / [F_{adh}(pH(3)) - F_{adh}(pH(11))].$$

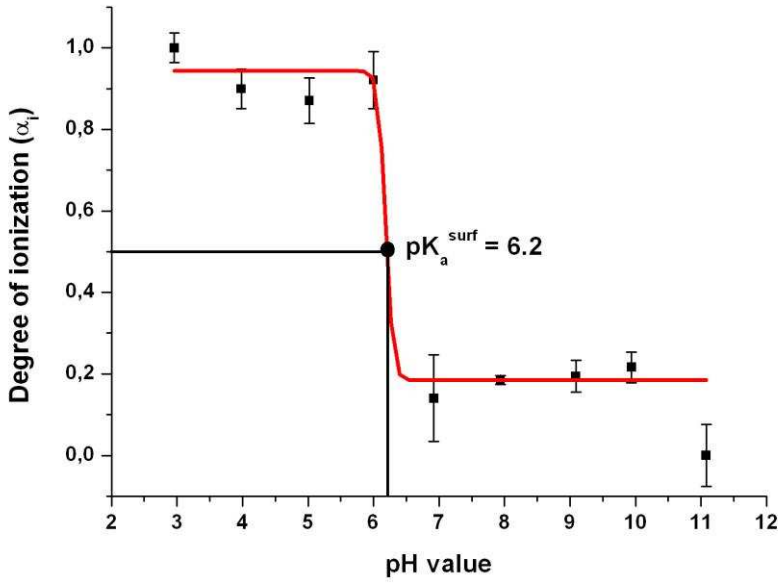

Figure 5. Degree of ionization α_i as a function of the pH calculated on the basis of the adhesion forces (Fig. 4).

We can therefore use this equation to calculate the degree of ionization for amino groups from the adhesion force values presented in Figure 4. Variations in surface ionization are presented in Figure 5. It can be used to determine the acid dissociation constant pK_a, defined as the pH at which α_i = ½. Experimentally, the surfacial amino groups' pK_a (i.e. pK_a^{surf}) is estimated at a value of 6.2, close to the value deduced from contact angle titration. Hence, local force microscopy measurements using modified AFM probes and macroscopic wetting studies

provide very similar values for the pKa of the surface amino groups. We can however notice that the pK_a^{surf} obtained shifts of about 4-5 pH units to lower pK_a values compared to the pK_a of free organic primary amines (pK_a ~ 10-11) [35, 42] in aqueous solution. Similar shifts to lower values were previously observed experimentally and related to the hydrophobicity of the local environment of the corresponding functional groups. Results indicate that the local environment of amino groups in the coating is somewhat hydrophobic. Upon lowering the pH, NH_2 groups will resist protonation since stabilisation of the charge is low in the (hydrophobic) environment. This causes a shift of the pK_a^{surf} to lower value. In general, this interpretation is corroborated by simulations [43].

Conclusion

In conclusion, we demonstrated a new, fast, reproducible technique to atomic force microscopy (AFM) tip functionalization for chemical interactions measurement. PECVD deposited amino-coatings were extensively characterised using XPS, AFM, contact angle, ellispometry and DPI measurements. Data highlighted the deposition, surface characteristics and stability of the coating. Moreover, a high amount of amine functional groups at coating surface was revealed. Their application in chemical interaction measurements through chemical force titration particularly demonstrated the successful functionalization of AFM tips as well as their stability and use under different environmental conditions.

Acknowledgment

This material is based upon works supported by the Science Foundation Ireland under Grant No. 05/CE3/B754. C.V. is a postdoctoral researcher of the Belgian Fund for Scientific Research (F.R.S. / F.N.R.S.). D.E.W. is an E.T.S. Walton visiting fellow of Science Foundation Ireland.

References

[1] Y. Sugimoto, P. Pou, M. Abe, P. Jelinek, R. Perez, S. Morita, O. Custance, Nature 446 (2007) 64; R. McKendry, M.-E. Theoclitou, T. Rayment, C. Abell, Nature 1998, 391, 566; R.W. Friddle, M.C. Lemieux, G. Cicero, A.B. Artyukhin, V.V. Tsukruk, J.C. Grossman, G. Galli, A. Noy, Nat. Nanotechnol. 2 (2007) 692.

[2] B. Bhushan, J.N. Israelachvili, U. Landman, Nature 374 (2002) 607; M. Fiebig, Th. Lottermoser, D. Fröhlich, A.V. Goltsev, R.V. Pisarev, Nature 419 (2002) 818.

[3] Y.F. Dufrêne, Nat. Rev. Microbiol. 2004, 2, 451; C. Volcke, S. Pirotton, Ch. Grandfils, C. Humbert, P.A. Thiry, I. Ydens, P. Dubois, M. Raes, J. Biotechnol. 125 (2006) 11.

[4] A.R. Kirby, A.P. Gunning, V.J. Morris, Trends Food Sci. Tech. 6 (1995) 359.

[5] K. Salaita, Y. Wang, C.A. Mirkin, Nat. Nanotechnol. 2 (2007) 145; A.M. Moulin, S.J. O'Shea, M.E. Welland, Ultramicroscopy 82 (2000) 23; C. Grogan, R. Raiteri, G.M. O'Connor, T.J. Glynn, V. Cunningham, M. Kane, M. Charlton, D. Leech, Biosens. Bioelectron. 17 (2002) 201.

[6] C. Grégoire, S. Marco, J. Thimonier, L. Duplan, E. Laurine, J.-P. Chauvin, B. Michel, V. Peyrot, J.M. Verdier, EMBO J. 20 (2001) 3313.

[7] G. Binnig, H. Rohrer, C. Gerber, E. Weibel, Phys. Rev. Lett. 49 (1982) 57; Binnig, H. Rohrer, C. Gerber, E. Weibel, Appl. Phys. Lett. 40 (1982) 178; G. Binnig, H. Rohrer, Helv. Phys. Acta 55 (1982) 726; G. Binnig, C.F. Quate, Ch. Gerber, Phys. Rev. Lett. 56 (1986) 930.

[8] R.M. Overney, E. Meyer, J. Frommer, D. Brodbeck, R. Luthi, L. Howald, H.J. Guntherodt, M. Fujihira, H. Takano, Y. Gotoh, Nature 359 (1992) 133; D.R. Baselt, J.D. Baldeschwieler, J. Vac. Sci. Technol. B 10 (1992) 2316.

[9] C.D. Frisbie, L.F. Rozsnyai, A. Noy, M.S. Wrighton, C.M. Lieber, Science 265 (1994) 2071.

[10] F. Bergasa, J.J. Saenz, Ultramicroscopy 42 (1992) 1189; Y. Leng, C.C. Williams, Colloid Surf. A-Physicochem. Eng. Asp. 93 (1994) 335; J.J. Saenz, N. Garcia, J.C. Slonczewski, Appl. Phys. Lett. 53 (1988) 1449; H.J. Mamin, D. Rugar, J.E. Stern, R.E. Fontana, P. Kasiraj, Appl. Phys. Lett. 55 (1989) 318.

[11] M. Rief, F. Oesterhelt, B. Heymann, H.E. Gaub, Science 275 (1997) 1295; S.P. Jarvis, S.I. Yamamoto, H. Yamada, H. Tokumoto, J.B. Pethica, Appl. Phys. Lett. 70 (1997) 2238.

[12] A.K. Henning, T. Hochwitz, J. Slinkman, J. Never, S. Hoffmann, P. Kaszuba, C. Daghlian, J. Appl. Phys. 77 (1995) 1888; C. Sommerhalter, T.W. Matthes, T. Glatzel, A. Jager-Waldau, M.C. Lux-Steiner, Appl. Phys. Lett. 75 (1999) 286.

[13] V.P. Pastushenko, P. Hinterdorfer, F. Kienberger, C. Borken, H. Schindler, Single Molecules 1 (2000) 165.

[14] P. Hinterdorfer, Y.F. Dufrêne, Nat. Methods 3 (2006) 347.

[15] T. Ito, P. Bühlmann, Y. Umezawa, Anal. Chem. 70 (1998) 255; T. Ito, P. Bühlmann, Y. Umezawa, Anal. Chem. 71 (1999) 1699; C.Volcke, P. Simonis, F. Durant, P.A. Thiry, P. Lambin, C. Culot, C. Humbert, Chem. Eur. J. 11 (2005) 4185; C.Volcke, P. Simonis, P.A. Thiry, P. Lambin, C. Culot, C. Humbert, Nanotechnology 6 (2005) 2596; C. Volcke, P. Simonis, F. Durant, P.A. Thiry, P. Lambin, C. Culot, C. Humbert, Physicalia Magazine 27 (2005) 415; C. Volcke, P.A. Thiry, J. Phys. – Conf. Series 61 (2007) 1236; C. Volcke, P. Simonis, C. Humbert, P. Lambin, C. Culot, P.A. Thiry, Phys. Chem. News 36 (2007) 34.

[16] S. Chang, J. He, A. Kibel, M. Lee, O. Sankey, P. Zhand, S. Lindsay, Nat. Nanotechnol. 4 (2009) 297.

[17] A. Noy, Surf. Interface Anal. 38 (2006) 1429.

[18] A.S. Duwez, U. Jonas, H. Klein, ChemPhysChem 4 (2003) 1107; B.D. Beake, G.J. Legget, Phys. Chem. Chem. Phys. 1 (1999) 3345; M.L. Carot, V.A. Macagno, P. Paredes-Olivera, E.M. Patrito, J. Phys. Chem. C 111 (2007) 4294.

[19] H. Kim, J. Noh, M. Hara, H. Lee, Ultramicroscopy 108 (2008) 1140; H. Kim, J.H. Park, I.-H. Cho, S.-K. Kim, S.-H. Paek, H. Lee, J. Colloid Interf. Sci. 334 (2009) 161; F. Sato, H. Okui, U. Akiba, K. Suga, M. Fujihira, Ultramicroscopy 97 (2003) 303; A.-S. Duwez, B. Nysten, Langmuir 17 (2001) 8287; P.D. Ashby, C.M. Lieber, J. Am. Chem. Soc. 127 (2005) 6814; M.A. Poggi, P.T. Lillehei, L.A. Bottomley, Chem. Mater. 17 (2005) 4289; A. Noy, C.D. Frisbie, L.F. Rozsnyai, M.S. Wrighton, C.M. Lieber, J. Am. Chem. Soc. 117 (1995) 7943.

[20] T. Ito, M. Namba, P. Bühlmann, Y. Umezawa, Langmuir 13 (1997) 4323.

[21] P. Favia, M. Creatore, F. Palumbo, V. Colaprico and R. d'Agostino Surf. Coat. Technol. 142-144 (2001) 1; H. Muguruma, Y. Kase Biosens.Bioelectron. 22 (2006) 737.

[22] R.P. Gandhiraman, S. Daniels, D.C. Cameron, B.P. McNamara, E. Tully, R. O'Kennedy, Surf. Coat. Technol. 200 (2005) 1031; R.P. Gandhiraman, S. Daniels, D.C. Cameron. Plasma Process. Polym. 4 (2007) 369; M.M. Dudek, R. P. Gandhiraman, C. Volcke, S. Daniels, A. J. Killard, Plasma Process. Polym. 6 (2009) 620; A. Riaz, R.P. Gandhiraman, I.K. Dimov, L.B. Desmonts, A.J. Ricco, J. Ducrée, S. Daniels, L.P. Lee, Proceedings of the 15th International Conference on Solid-State Sensors, Actuators & Microsystems (Transducers'09), June 21-25, Denver, Colorado, USA, pages 1051-1054, 2009.

[23] M.M. Dudek, R.P. Gandhiraman, C. Volcke, A.A. Cafolla, S. Daniels A.J. Killard, Langmuir 25 (2009) 11155.

[24] D. Jung, S. Yeo, J. Kim, B. Kim, B. Jin, D.-Y. Ryu, Surf. Coat. Technol. 200 (2006) 2886; K. Nakanishi, H.i Muguruma, I. Karube. Anal.Chem. 68 (1996) 1695.

[25] J. Kim, D. Jung, Y. Park, Y. Kim, D.W. Moon, T.G. Lee, Appl. Surf. Sci. 253 (2007) 4112.

[26] R.P. Gandhiraman, C. Volcke, V. Gubala, C. Doyle, L. Basabe-Desmonts, C. Dotzler, M.F. Toney, M. Iacono, R.I. Nooney, S. Daniels, B. James, D.E. Williams, J. Mat. Chem. (2010) accepted.

[27] C. Volcke, R.P. Gandhiraman, V. Gubala, J. Raj, Th. Cummins, G. Fonder, R.I. Nooney, Z. Mekhalif, G. Herzog, S. Daniels, D.W.M. Arrigan, A.A. Cafolla, D.E. Williams, Biosens. Bioelectron. (2010) DOI:10.1016/j.bios.2009.12.034.

[28] R.P. Gandhiraman, S.K. Karkari, S.M. Daniels, Brian McCraith. Surf. Coat. Technol. 203 (2009) 3521.

[29] M. Haïdopoulos, F. Mirabella, M. Horgnies, C. Volcke, P.A. Thiry, P. Rouxhet, J.-J. Pireaux, J. Microsc.-Oxf. 228 (2007) 227.

[30] Y. Cho, A. Ivanisevic, J. Phys. Chem. B 108 (2004) 15223.

[31] G. Beamson and D. Briggs, High resolution XPS of organic polymers: the Scienta ESCA300 database, Chichester, New York, 1992

[32] S. Fiorilli, P. rivolo, E. Descrovi, C. Ricciardi, L. Pasquardini, L. Lunelli, L. Vanzetti, C. Pederzolli, B. Onida, E. Garonne, J. Colloid Interf. Sci. 321 (2008) 235–241.

[33] M.L. Wallwork, D.A. Smith, Langmuir 17 (2001) 1126.

[34] H.-X. He, W. Hang, H. Zhang, Q.G. Li, S.F.Y. Li, Z.F. Liu, Langmuir 16 (2000) 517.

[35] H. Zhang, H.X. He, T. Mu, Z.-F. Liu, Thin Solid Films 327-329 (1998) 778.

[36] J. Zhang, J. Kirkham, C. Robinson, M.L. Wallwork, D.A. Smith, A. Marsh, M. Wong, Anal. Chem. 72 (2000) 1973.

[37] D.A. Smith, M.L. Wallwork, J. Zhang, J. Kirkham, C. Robinson, A. Marsh, M. Wong, J. Phys. Chem. B 104 (2000) 8862.

[38] J. Wang, H. Zhang, H. He, T. Hou, Z. Li, X. Xu, J. Mol. Struc. 451 (1998) 295; B. Wang, R.D. Oleschuk, J.H. Horton, Langmuir 21 (2005) 1290.

[39] A. Geissler, M.-F. Vallat, L. Vidal, J.-C. Voegel, J. Hemmerlé, P. Schaaf, V. Roucoules, Langmuir 24 (2008) 4874.

[40] D.V. Venezov, A. Noy, L.F. Rozsnyai, C.M. Lieber J. Am. Chem. Soc. 119 (1997) 2006.

[41] K.L. Johnson, K. Kendall, A.D. Roberts Proc. R. Soc. A 324 (1971) 301.

[42] E.W. van der Vegte, G. Hadziioannou J. Phys. Chem. B 101 (1997) 9563; H. Schönherr, M.T. van Os, Z. Hruska, J. Kurdi, R. Förch, F. Arefi-Khonsari, W. Knoll, G.J. Vancso, Chem Comm (2000) 1303.

[43] J.L. Smart, J.A. McCammon, J. Am. Chem. Soc. 118 (1996) 2283.

Figures

Figure 1: High resolution core level photoemission spectra of (a) C 1s (b) N 1s (c) Si 2p, taken with a pass energy of 20 eV using monochromatic Al Kα monochromatic X-rays (1486.69 eV), with the X-ray source operating at 100 W. The analysis area was a 220 by 220 micron spot. The measurements were carried out in normal emission geometry. The core level peaks are deconvoluted to show the various bonding environments. Data analysis was performed using CasaXPS (www.casaXPS.com). Shirley backgrounds were used in the peak fitting. Core level data were fitted using Gaussian-Lorentzian peaks (30 % Lorentzian).

Figure 2: Tapping-Mode AFM topographical imaging of PECVD deposited APTES coating on silicon wafer in diverse environment: (A) in air, (B) in DI water, (C) in PBS Tween®, (D) in air after washing with DI water and drying in air, (E) in air after washing with PBS Tween® and drying in air. RMS roughness values are also indicated.

Figure 3: Representative force curves (approach in black and retraction in red) for NH_2 terminated tips and NH_2 modified substrate surface in different pH solutions. Upper number indicates pH of the solution during experiment.

Figure 4: Chemical force titration curve for tip and surface both modified with PECVD deposited APTES coating, acquired under solution of 10^{-2} M ionic strength. (The curve has been added as a guide to the eye). Scheme are presenting the proposed interactions of APTES modified tips and APTES modified surface in water at different pH values. (B) Negative cosine of the averaged contact angles of water drops on a silicon surface modified with PECVD deposited APTES as a function of pH

Figure 5: Degree of ionization α_i as a function of the pH calculated on the basis of the adhesion forces (Fig. 4).

5: Figure 1

Click here to download high resolution image

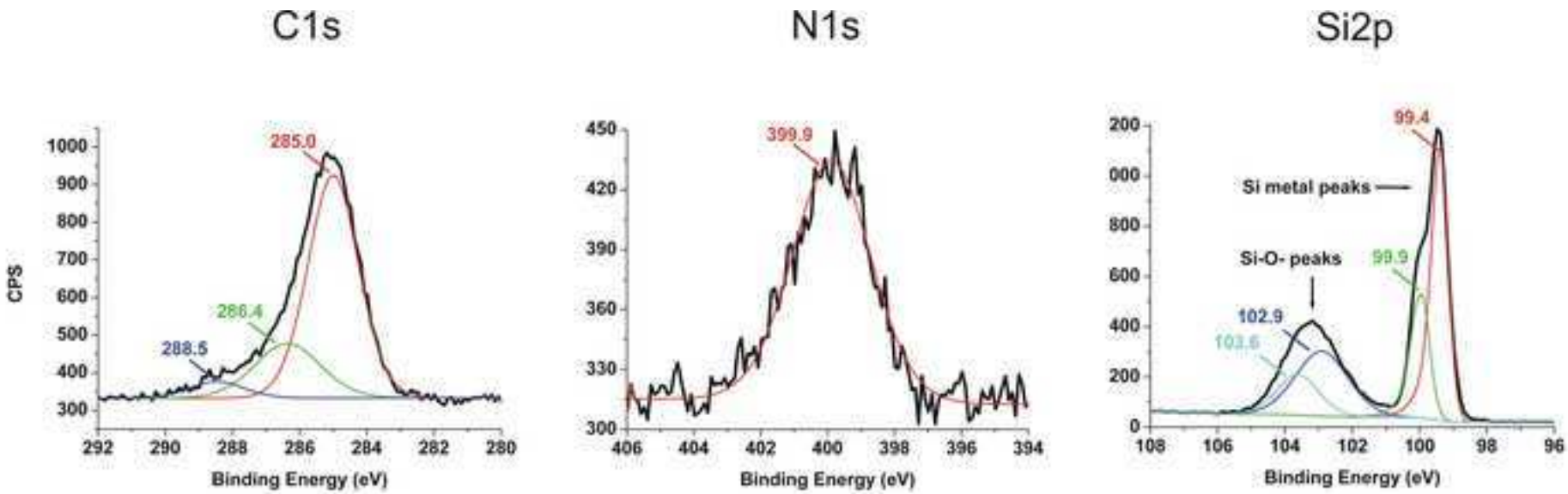

5: Figure 2
Click here to download high resolution image

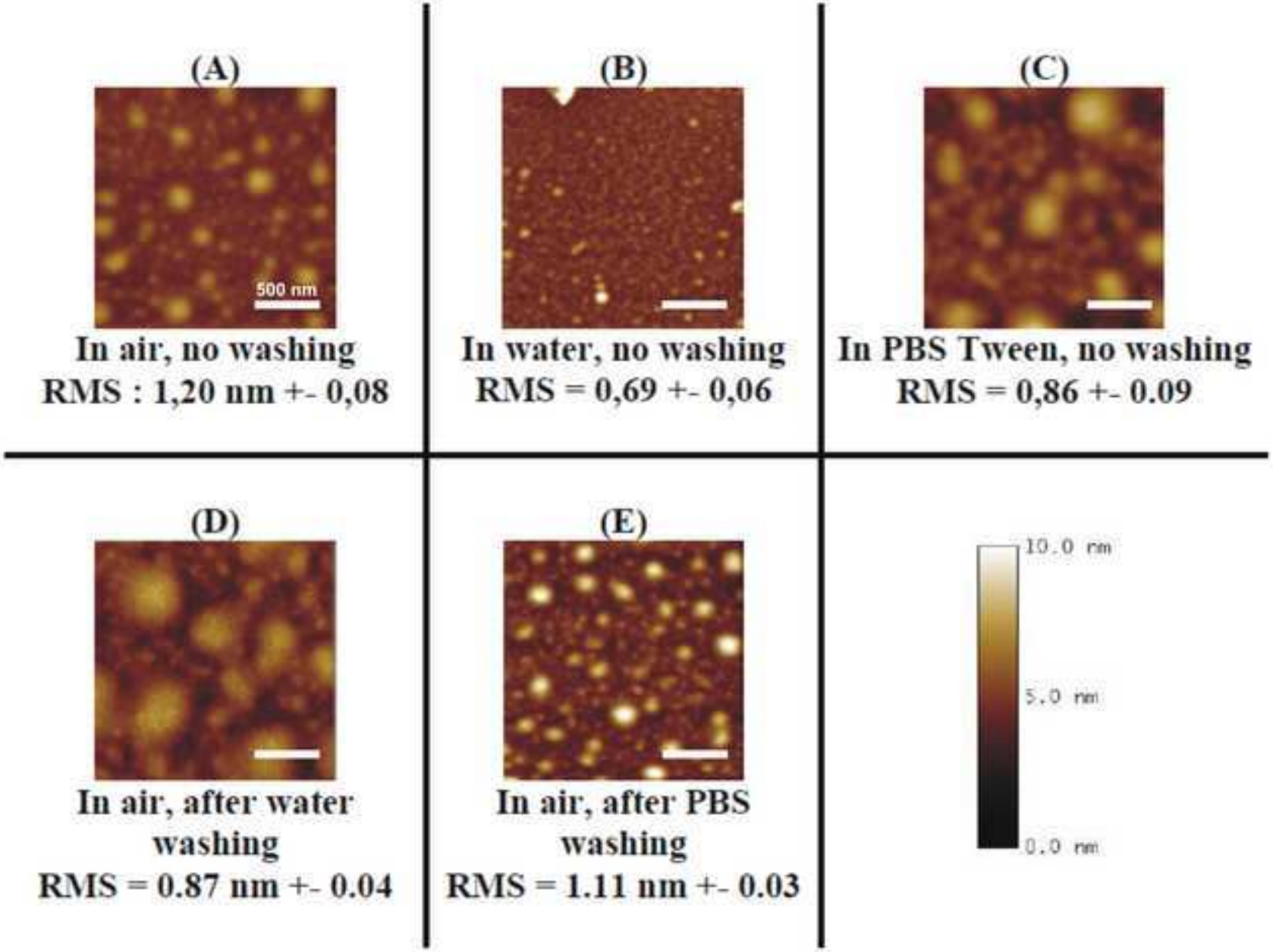

5: Figure 3

Click here to download high resolution image

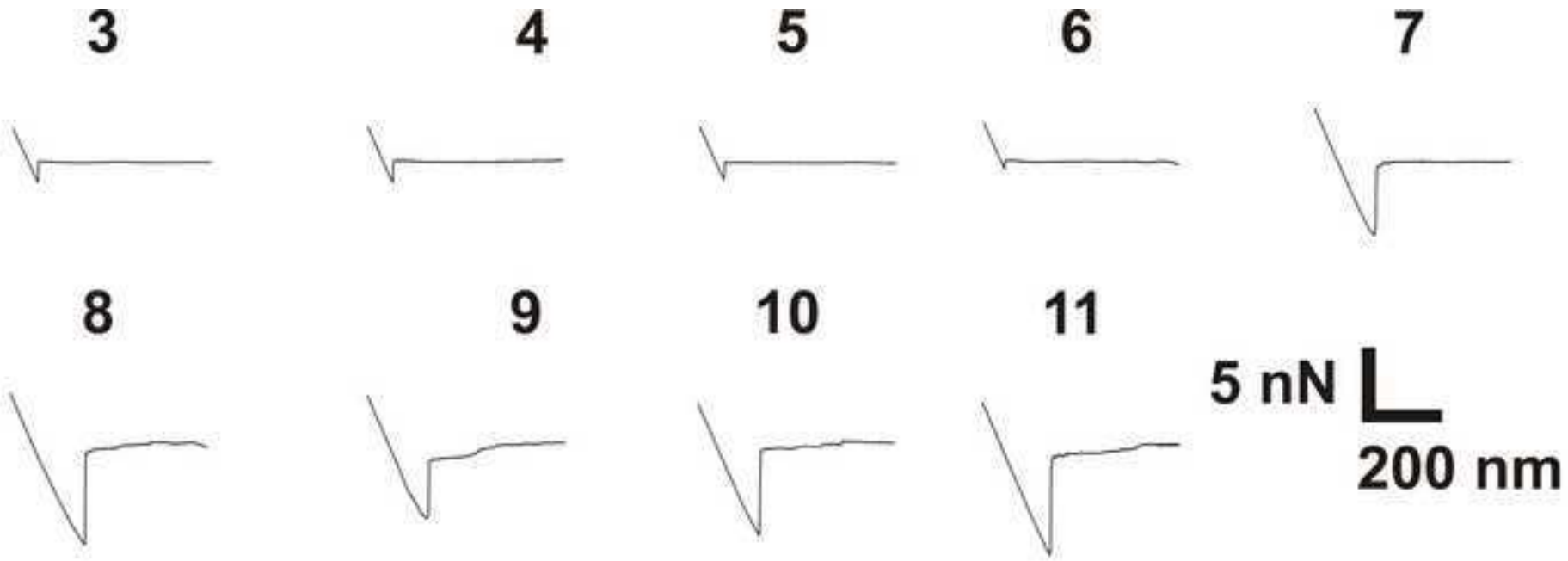

5: Figure 4

Click here to download high resolution image

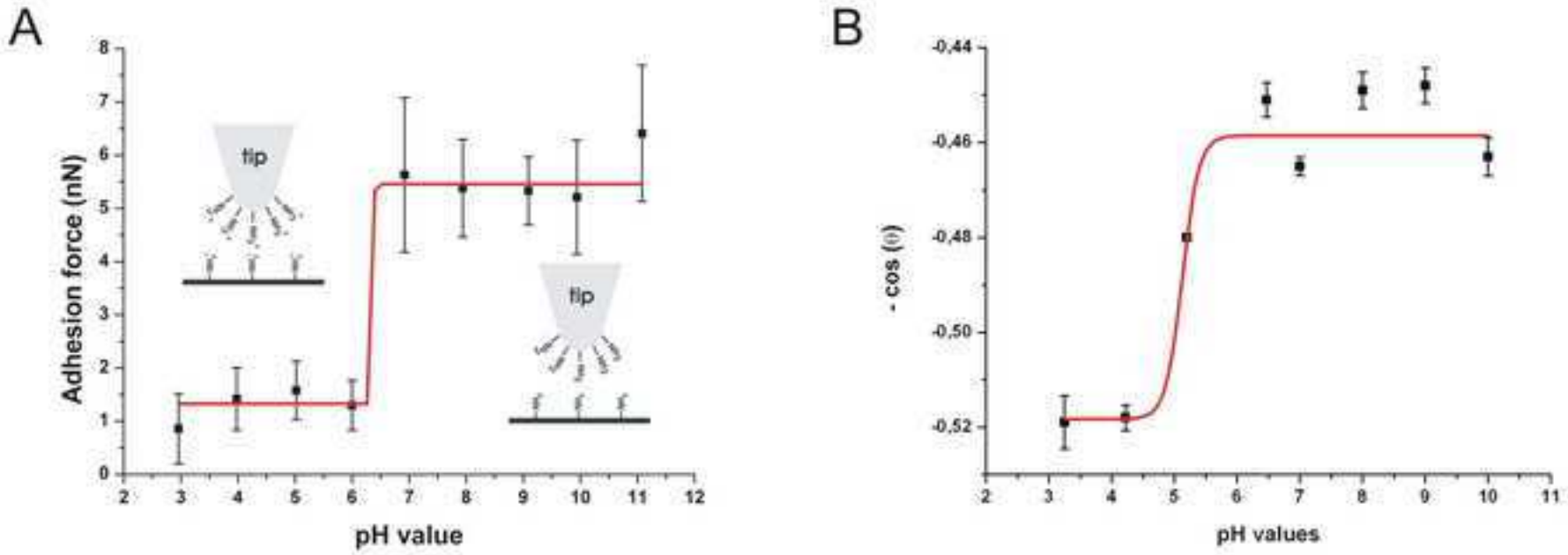

5: Figure 5
Click here to download high resolution image

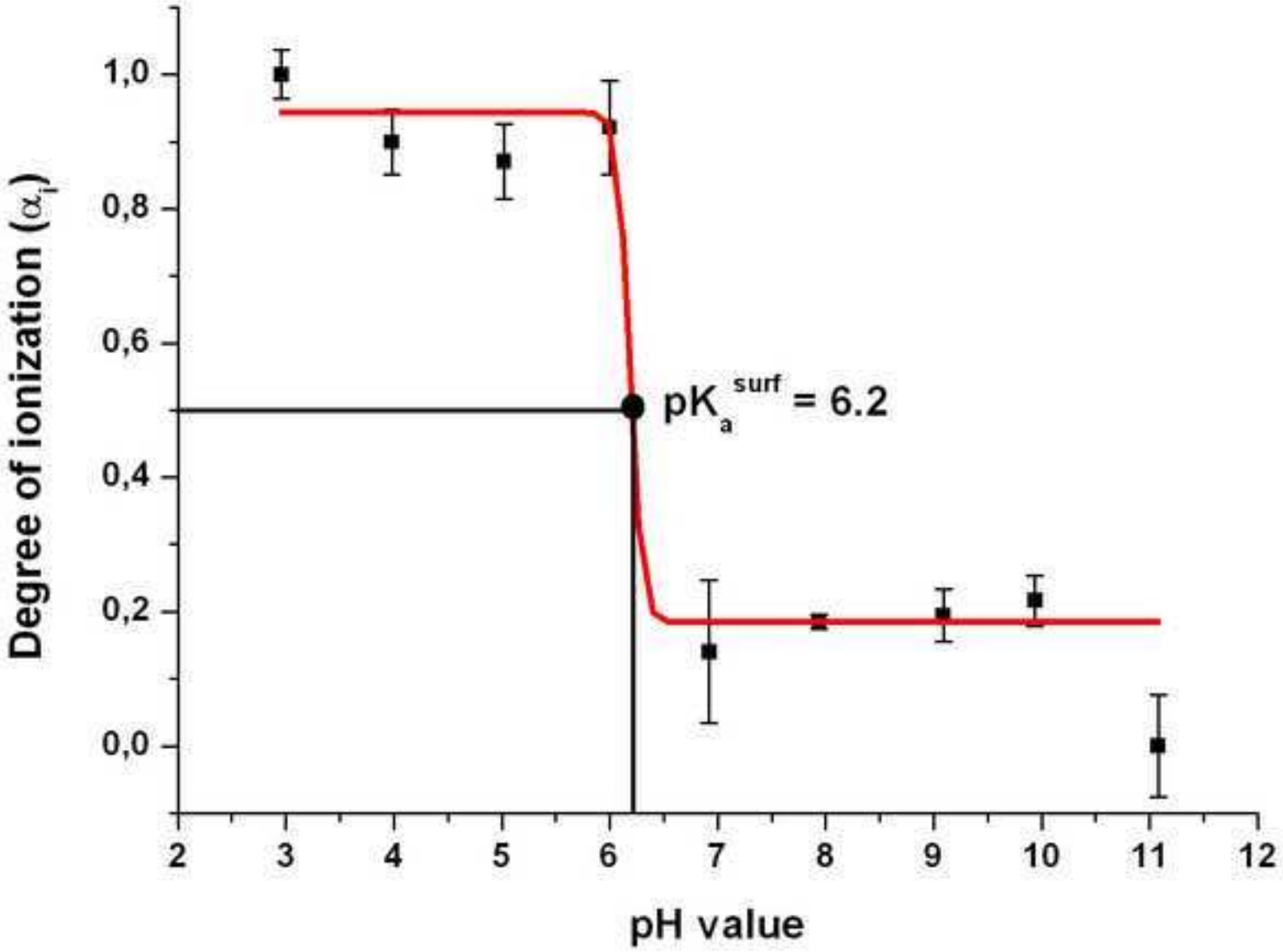

7: Electronic Supplementary Material (online publication only)

Click here to download 7: Electronic Supplementary Material (online publication only): Supporting Informations.pdf